Neurochemistry International

Synergistic Ca^{2+} and Cu^{2+} requirements of the FGF1-S100A13 interaction measured by quartz crystal microbalance: an initial step in amlexanox-reversible non-classical release of FGF1

Hayato Matsunaga, Hiroshi Ueda*

Division of Molecular Pharmacology and Neuroscience, Nagasaki University Graduate School of Biomedical Sciences, 1-14 Bunkyo-machi, Nagasaki 852-8521, Japan

*Address correspondence and reprint requests to Dr. Hiroshi Ueda,
Division of Molecular Pharmacology and Neuroscience, Nagasaki University Graduate School of Biomedical Sciences, 1-14 Bunkyo-machi, Nagasaki 852-8521, Japan.
Tel: +81-95-819-2421; Fax: +81-95-819-2420; E-mail: ueda@nagasaki-u.ac.jp

Footnotes

Running Title: Metal ion regulation of the FGF1-S100A13 interaction

Abbreviations: FGF1, fibroblast growth factor-1; EC_{50}, median effective concentration; k_a, association rate constant; K_D, dissociation constant; K_i, inhibition constant; Cys, cysteine; QCM, quartz crystal microbalance; GST, glutathione S-transferase; MW, molecular weight; IL, interleukin; EGTA, ethyleneglycol bis (2-aminoethylether) tetraacetic acid; CICR, Ca^{2+}-induced Ca^{2+} release; His, histidine; Glu, glutamic acid.

Abstract

It is known that fibroblast growth factor-1 (FGF1) lacking a conventional signal peptide sequence shows non-classical release independent of the endoplasmic reticulum-Golgi system. Recent studies reveal that FGF1 is co-released with S100A13, a Ca^{2+}-binding protein that acts as an extracellular cargo molecule. Although both FGF1 and S100A13 are Cu^{2+}-binding proteins, the role of Cu^{2+}, as well as that of Ca^{2+}, in non-classical release, remains to be clarified. In the present study we examined the requirements of both metal ions for the interaction between these two proteins. The addition of Ca^{2+} significantly increased the k_a value, while decreasing the K_D value, for the interaction between *Strep*-tagII-S100A13 and GST-FGF1; both values were obtained by use of a quartz crystal microbalance, a real-time mass measuring device. The EC_{50} of Ca^{2+} to enhance the interaction was 10.11 μM. Although the addition of Cu^{2+} alone had no effect, it caused a marked potentiation of the Ca^{2+}-enhanced interaction. The EC_{50} of Cu^{2+} for the potentiation was 50.45 nM. On the other hand, the EC_{50} of Ca^{2+} and the K_D value were decreased from 11.69 to 2.07 μM and 0.75 to 0.38 x 10^{-7} M, respectively, by the addition of 200 nM Cu^{2+}. The Cu^{2+}–induced potentiation of this interaction was abolished by amlexanox, which inhibits non-classical release of FGF1. All of these findings suggest that synergistic effects of Ca^{2+} and Cu^{2+} play a key role in the interaction between FGF1 and S100A13, which is the initial step in non-classical release of FGF1.

Keywords: FGF1; S100A13; Non-classical release; Quartz crystal microbalance; Amlexanox; Protein-protein interaction.

1. Introduction

Fibroblast growth factor-1 (FGF1) has a multitude of biological activities. During development, FGF1 regulates the induction of neurulation and mesodermal induction, and the formation of circulatory and skeletal systems (Friesel and Maciag, 1999). This protein also plays important roles in neuroprotection, neurogenesis, tissue regeneration, angiogenesis, inflammation and the formation of some tumors in adulthood (Friesel and Maciag, 1999; Reuss and von Bohlen und Halbach, 2003). Thus, it is evident that FGF1 has a vast number of biological actions. However, the molecular machineries underlying the secretion of FGF1 remain to be determined, since known endoplasmic reticulum-Golgi-dependent vesicular (or classical) release upon cell stimulation is unlikely to be the case with FGF1, which lacks a conventional signal peptide sequence at its amino terminus (Cleves, 1997; Nickel, 2003; Prudovsky et al., 2003). Limited current studies have revealed that the formation of a multi-protein complex consisting of FGF1, S100A13 and the p40 form of synaptotagmin-1 is a crucial step for stress-induced FGF1 release (Tarantini et al., 1998; LaVallee et al., 1998; Landriscina et al., 2001b). Recently, we found that S100A13 is co-released with FGF1 from brain astrocytes subjected to starvation stress, and this protein behaves as a cargo molecule in this stress-induced non-classical FGF1 release (Matsunaga and Ueda, 2006a).

S100A13 belongs to the largest family of Ca^{2+}-binding S100 proteins, having an EF-hand peptide sequence (Bhattacharya et al., 2004; Sivaraja et al., 2005). S100 proteins show cell- and tissue-specific expression throughout the body, and play important roles in development, differentiation and tumor formation (Heizmann et al., 2002; Zimmer et al., 2003). However, S100A13 has some different characteristics from

other S100s, as observed in its ubiquitous expression throughout the body (Ridinger et al., 2000; Chan et al., 2003). This suggests that S100A13 may have general roles in cell signaling. Another characteristic difference is found in its Ca^{2+}-binding sites. Typical S100s are present in dimeric form and have four cooperative Ca^{2+}-binding sites, whereas monomeric S100A13 has only two Ca^{2+}-binding sites, of different affinity (Sivaraja et al., 2005). Recently, we demonstrated that S100A13 plays a role as a cargo molecule for Ca^{2+}-dependent non-classical release of FGF1 (Matsunaga and Ueda, 2006a and b).

On the other hand, it is reported that dimeric S100A13 also has two Cu^{2+}-binding sites with equivalent affinity to the Ca^{2+}-binding sites (Arnesano et al., 2005; Sivaraja et al., 2006). This unique nature may be related to the fact that S100A13 has only two Ca^{2+}-binding sites, unlike other S100 family proteins. It should be noted that FGF1 also has Cu^{2+}-binding affinity and that the depletion of intracellular Cu^{2+} by a specific chelating agent prevents stress-induced FGF1 release (Landriscina et al., 2001a; Matsunaga and Ueda, 2006a and b). Furthermore, it is also reported that the homodimerization and non-classical release of FGF1 are closely related to the Cu^{2+}-mediated oxidation of cysteine (Cys) 30 (Jackson et al., 1995; Tarantini et al., 1995). These findings suggest that S100A13 and FGF1 may form a heterooligomer, holding Cu^{2+} inside.

However, little is known of molecular machinery underlying the Cu^{2+}- and Ca^{2+}-mediated regulation of the interaction between FGF1 and S100A13, which is the initial step in non-classical release of FGF1. Here, we report a new approach to analyze the interplay of Ca^{2+} and Cu^{2+} in the FGF1-S100A13 interaction by use of a quartz

crystal microbalance (QCM), a real-time mass-measuring biosensor for examining protein-protein interactions.

2. Experimental Procedures

2.1. Materials

Amlexanox was kindly provided by Takeda Pharmaceutical Company Limited (Osaka, Japan).

2.2. Expression constructs and purification of recombinant proteins

The plasmid constructions of rat FGF1 and S100A13, and the purification of recombinant proteins have been described previously (Matsunaga and Ueda, 2006a). The FGF1 and S100A13 genes were cloned into the pGEX-5X-1 (GE Healthcare Bio-Sciences Corp., Piscataway, NJ) and pASK-IBA7 (Genosys Biotechnologies, Inc., Woodlands, TX) expression vectors, respectively. Recombinant GST-FGF1 protein was purified by Glutathione-Sepharose™ (GE Healthcare Bio-Sciences Corp.). Purified GST-FGF1 was confirmed to have equivalent extracellular activity to the native one (data not shown). Recombinant *Strep*-tagII-S100A13 (full-length and Δ88-98) proteins were purified using *Strep*-Tactin™-Sepharose (Genosys Biotechnologies, Inc.). In the former recombinant protein, *Strep*-tagII is the tag peptide, consisting of 8 amino acids. In some experiments we used tag-free recombinant proteins, FGF1 and S100A13, retaining GIPEF and RDRGPEF as amino terminal residues, respectively by digesting GST-FGF1 and *Strep*-tagII-S100A13 with Factor Xa (Boehringer Mannheim GmbH, Mannheim, Germany) for 12 h at 20°C. GST-tag and *Strep*-tagII were first removed using Glutathione-Sepharose™ and *Strep*-Tactin™-Sepharose, respectively, and Factor Xa was then removed by molecular exclusion chromatography using Ultrafree®-MC 30,000 NMWL centrifugal filter unit (Millipore, Bedford, MA). For the analysis of protein-protein interaction and its modulation by ions, we adopted the following

molecular weight values (average mass) for GST-FGF1, *Strep*-tagII-S100A13 full-length, its Δ88-98 mutant protein, tag-free S100A13, Ca and Cu: 44212.75, 13840.08, 12490.08, 12055.78, 40.078 and 63.546, respectively.

2.3. Gravimetric measurements with a biosensor quartz crystal microbalance (QCM)

AT-cut quartz crystals with a fundamental frequency of 27 MHz were purchased from Initium Inc. (Tokyo, Japan), and coated with a thin gold surface layer (effective surface area, 4.9 mm^2). Immediately before use, the gold surface of the quartz resonator was cleaned with piranha solution (H_2SO_4: 30% H_2O_2=3:1) for 5 min, and thoroughly washed with double-distilled water. An anti-GST antibody (GE Healthcare Bio-Sciences Corp.) was applied to the resonator for 30 min to obtain a layer for the immobilization of GST-FGF1. Next, the resonator was rinsed with interaction buffer (50 mM Tris-HCl pH 7.6, 15 mM NaCl, 140 mM KCl), immersed in interaction buffer (8 ml), subjected to immobilization of GST-FGF1 for 30 min, and then placed in fresh interaction buffer. Protein-protein interactions were detected using an AffinixQ system (Initium Inc.), a QCM sensor device. The interactions were determined from the frequency changes (oscillation unit, OU: -ΔF in Hz) due to changes in the mass on the electrode at the sub-nanogram level, upon application of a small volume (1 – 10 μl) of protein solution. From the Sauerbrey formula, an increase of 1 Hz OU is calculated as an interaction of a molecule of 30.38 pg with the biosensor. In all immobilization of GST-FGF1 on the resonator, it was confirmed that approximately 275 femtomoles of GST-FGF1 was immobilized as an absolute amount (an increase in OU of 400 Hz). All experiments were carried out at 25 ± 1 °C. All sensorgram data show the OU value following the association phase. For equilibrium analysis based on the Langmuir

binding model, frequency changes induced by applied protein at any concentration were curve-fitted to the linear-reciprocal plot: $X/B = [X]/B_{max} + K_D/B_{max}$. X and B denote the concentration of the added protein and the mass level bound to the immobilized protein, respectively. For kinetic analysis, frequency changes induced by cumulatively applied protein were curve-fitted to the formula $\Delta F=A(e^{(-1/\tau)T}-1)$, and the $1/\tau$ value was plotted for each concentration of added protein. $1/\tau$ and K_D represent $k_a[X] + k_d$ and k_d/k_a, respectively, where X is the concentration of the added protein. To determine the inhibitory activity of amlexanox against FGF1-S100A13 interaction, we calculated inhibition constant (K_i value). The τ (relaxation time) value was plotted against each concentration of Amlexanox. The Dixon plot gives an intersection point from all linear-curves by several concentrations of *Strep*-tagII-S100A13, and this x-coordinate represents - K_i.

2.4. Statistical analysis

All results are shown as means $\pm$ S.E.M. Two-independent groups were compared using a Student's *t*-test. Multigroups were compared using Dunnett's multiple comparison test after a one-factor ANOVA. $p < 0.05$ was considered significant.

3. Results

3.1. Interaction between FGF1 and S100A13 evaluated by biosensor QCM

A QCM is a very sensitive mass-measuring device for studying protein-protein interactions. To characterize the interaction between FGF1 and S100A13, we prepared mutants of both proteins as GST- and *Strep*-tagII-fusion proteins, respectively. Biosensor was first immobilized with GST-FGF1, and immersed in interaction buffer containing divalent metal-ions, 500 μM Mg^{2+}, 100 nM Ca^{2+} and 200 nM Cu^{2+} to wait for the stabilization of basal quartz oscillation. When *Strep*-tagII-S100A13 at a concentration of 200 nM was added to the cuvette, the reactive oscillation units (OU: -ΔF in Hz) were slightly increased, and reached a plateau (11 OU) after 5 – 10 min (Fig. 1A). Elevation of Ca^{2+} rapidly increased the OU in a Ca^{2+} concentration-dependent manner (10 – 100 μM, final concentration), while further addition of 2 mM EGTA reversed this increase. Complete reversal was observed in the cases with 10 and 30 μM Ca^{2+}. These results suggest the enhancement of interaction between GST-FGF1 and *Strep*-tagII-S100A13 is Ca^{2+}-dependent.

We already reported that the *Strep*-tagII-S100A13 C-terminal deletion mutant (Δ88-98) shows no interaction with GST-FGF1 in a pull-down assay (Matsunaga and Ueda, 2006a). The C-terminal 11 amino acids of S100A13 (RKEKVLAIRKK) include six basic amino acids (Fig. 1B), a structure that is unique among S100s (Donato, 1999). As shown in Fig. 2C, the addition of Δ88-98 mutant to GST-FGF1 showed no significant interaction in the QCM assay, while subsequent addition of full-length S100A13 did (Fig. 1C).

3.2. Reduced interaction of Strep-tagII-S100A13 heterodimer of full-length and C-terminal deletion mutant with GST-FGF1

To characterize the C-terminal region in terms of its interaction with FGF1, the QCM assay was performed using a mixture of full-length and C-terminal deletion (Δ88-98) mutant *Strep*-tagII-S100A13, in comparison with preparations comprising full-length protein. The expected combinations of dimers in the mixture include a homodimer of full-length *Strep*-tagII-S100A13 [F:F], a heterodimer of full-length *Strep*-tagII-S100A13 and its deletion mutant [F:D], and a homodimer of deletion mutant [D:D] (Fig. 2A). The application of full-length S100A13 at 100 and 200 nM concentration-dependently increased the interaction with GST-FGF1 (275 femtomoles), as shown in Fig. 2Ba,b. The addition of deletion mutant (100 and 200 nM) also concentration-dependently increased the interaction by full-length protein (100 nM), but it was less potent than the full-length (Fig. 2Bd,e). This less potency was confirmed when the interaction using equimolar unitable dimers comprised of full-length plus mutant was compared to the case with full-length alone. As above-mentioned, the expected concentration as unitable dimers in the case with 75 nM full-length plus 75 nM mutant is the same as in the case with 100 nM full-length. As shown in Fig. 2Ba and c, the former combination with mutant showed slightly less potency than the latter without mutant. Similar slight change was also observed with 150 nM full-length plus 150 nM mutant *vs.* 200 nM full-length (Fig. 2Bb and f). In order to measure the stoichiometry of full-length and mutant proteins per GST-FGF1, combinations of these proteins at different ratios were adopted (Fig. 2C). The results (OU values) were converted to the weight of proteins bound to GST-FGF1, using the fact that an increase of 1 OU corresponds to 30.38 pg. In our analysis, we assume that the potency to

dimerize is similar among S100A13 species ([F:F], [F:D] and [D:D]) from the fact that deletion mutants lacking C-terminal region of other members of S100 protein family retain the same potency to dimerize (Osterloh et al., 1998; Donato, 1999). The mixture of full-length plus deletion mutant (1:1) comprises 1/3 [F:F], 1/3 [F:D] and 1/3 [D:D], as indicated in Fig. 2C. As the [D:D] dimer is unable to interact with GST-FGF1, it was not counted toward further analysis (Fig. 2D). The linear curve (double-reciprocal plot) from the sample containing full-length protein only represents $X/B = [X]/B_{max} + K_D/B_{max}$ (X: concentration of [F:F] and [F:D] dimers). The K_D value of [F:F] for GST-FGF1 was calculated as 0.915×10^{-7} M from this approximate formula. Plots obtained with different concentrations of full-length protein plus deletion mutant (1:1) show a slightly upper shifted linear curve, compared to the case with full-length protein alone (Fig. 2D). The loss of weight in deletion mutant is only ~10% of the full-length S100A13. In addition, as the mixture using this mutant comprises [F:F] and [F:D], the calculated loss seems to be only ~2.5% (the ratio of D in this mixture is only 1/4), if the affinity to FGF1 is the same between [F:F] and [F:D]. This finding indicates that the relative potency of [F:F] to interact with GST-FGF1 is higher than that of [F:D]. Assuming that the amount of [F:F] bound to GST-FGF1 is [a], while the amount of [F:D] bound to GST-FGF1 is [b], the following formula can be derived: the weight of bound S100A13 species = $[F:F]_{MW} \times [a/(a + b)] + [F:D]_{MW} \times [b/(a + b)]$. When the weight values, 29.55, 34.96, and 38.85 obtained in Fig. 2C were incorporated into the formula, the bound ratio ([F:D]/[F:F] = b/a) was calculated as 0.50 ± 0.00. Therefore, the final estimation of the loss of weight of protein plus deletion mutant (1:1) is expected to be only ~1.25% compared to the weight of bound full-length protein alone.

3.3. Kinetic analysis of Ca^{2+}-dependent interaction

To examine the Ca^{2+}-specificity of the enhancement of interaction between GST-FGF1 and *Strep*-tagII-S100A13, Cu^{2+} and Mg^{2+} were omitted from the interaction buffer. As shown in Fig. 3A, the interaction was enhanced in a Ca^{2+} concentration-dependent manner in the range between 3 and 200 μM, while no more enhancement was observed with 500 μM. However, no enhancement was observed with 200 nM Cu^{2+} or 500 μM Mg^{2+}. The OU in the presence of various concentrations of Ca^{2+} (3 – 700 μM) showed an equilibration at 10 min. When the OU obtained at 10 min (Fig. 3A) was plotted against each Ca^{2+} concentration, the fitted curve appeared to confirm to Michaelis-Menten kinetics (Fig. 3B). In the linear curve by Hanes-Woolf plot, the slope denotes 1/ OU_{max} (Fig. 3C). OU_{max} and OU_{50} were 83.33 and 41.67, respectively. From the formula indicated in Fig. 3B, the EC_{50} of Ca^{2+} for the interaction between GST-FGF1 and *Strep*-tagII-S100A13 was calculated as 10.11 μM. Cumulative applications of *Strep*-tagII-S100A13 showed step-wise increases in OU in the presence of 100 μM Ca^{2+} (Fig. 3D). The plot of $1/\tau$ value against different concentrations of *Strep*-tagII-S100A13 showed a linear curve both in the absence or presence of 100 μM Ca^{2+} (Fig. 3E). From the kinetics, the addition of Ca^{2+} increased the k_a, and decreased the K_D (Fig. 3F and G).

3.4. Cu^{2+}-induced potentiation of Ca^{2+}-dependent interaction

To examine the effect of Cu^{2+} on the interaction, the concentrations of Cu^{2+} were varied in the presence of 100 μM Ca^{2+} and 500 μM of Mg^{2+} (Fig. 4A). In the absence of Cu^{2+}, the OU value was 68.7 at 10 min, which is equivalent to the value in the presence of 100 μM Ca^{2+} alone. The addition of Cu^{2+} concentration-dependently

potentiated the Ca^{2+}-dependent increase in OU, in the range of 10 – 200 nM. No additional increase in OU was induced by 500 nM Cu^{2+} (data not shown). From the kinetics using Cu^{2+}-potentiated OU (ΔOU), as mentioned above, the EC_{50} of Cu^{2+} to potentiate the Ca^{2+}-dependent increase was calculated as 50.45 nM (Fig. 4B and C).

When the interaction under the condition of various concentrations of Ca^{2+} was analyzed by Michaelis-Menten kinetics and Hanes-Woolf plot, the EC_{50} was calculated as 11.69 μM and 2.07 μM, and the OU_{max} was 83.33 and 125.00 Hz, in the absence and presence of 200 nM Cu^{2+}, respectively (Fig. 4D and E). Kinetic analyses using cumulative applications of S100A13 also demonstrated the significant Ca^{2+} concentration-dependent increase in the interaction and synergistic effects by Cu^{2+} in terms of k_a and K_D (Table 1). Similar results were also observed in the interaction between tag-free recombinant proteins. Although the basal activity with tag-free proteins showed smaller k_a than that with tagged ones in the presence of 100 nM Ca^{2+} alone, the fold-changes in k_a by Ca^{2+} and Cu^{2+} were comparable between both cases.

Repeated experiments revealed that the average ± S.E.M. of OU in the presence of 100 μM Ca^{2+}, 200 nM Cu^{2+} and 500 μM of Mg^{2+}, equivalent to OU_{max}, was 128.95 ± 2.69 Hz (n=4), which corresponds to 3917.50 ± 81.71 pg, since 1 Hz OU is equivalent to 30.38 pg. On the other hand, the molecular weight of *Strep*-tagII-S100A13 holding respectively one and two molecules of Cu^{2+} and Ca^{2+} is calculated as 13983.78. As the amount of *Strep*-tagII-S100A13 bound to immobilized GST-FGF1 (275 femtomoles) on the biosensor was calculated as 280.15 ± 5.84 femtomoles, the stoichiometry of the interaction between both proteins appears to be 1:1.

3.5. Amlexanox-reversible Cu^{2+}-potentiation

As S100A13 protein has been identified as a target of the anti-allergic drug, amlexanox, which inhibits degranulation of mast cells and release of FGF1 and interleukin-1α (IL-1α) (Mouta Carreira et al., 1998; Shishibori et al., 1999; Mandinova et al., 2003), the effects of amlexanox on the interaction between GST-FGF1 and *Strep*-tagII-S100A13 were studied (Table 1). As mentioned above, a Ca^{2+}-dependent increase in k_a and decrease in K_D was observed in the absence of Cu^{2+}. The addition of 100 μM amlexanox had no effect on these values. The addition of Cu^{2+} increased k_a, while decreased K_D in the presence of 10^{-4} M Ca^{2+}, but not in the presence of 10^{-7} M Ca^{2+}. The potentiation by Cu^{2+} was abolished by the addition of amlexanox.

This reversal activity of amlexanox in the K_D decreased in the presence of 10^{-4} M Ca^{2+}, and 200 nM Cu^{2+} was concentration-dependent in the range of 100 nM to 100 μM (Fig. 5A). From the Dixon plot, K_i value of amlexanox was calculated as 2.38 $\pm$ 0.01 μM (Fig. 5B).

4. Discussion

Previously, we have successfully demonstrated that S100A13 is a cargo molecule for stress-induced non-classical release of FGF1, and that Ca^{2+} mobilization is involved in the interaction between FGF1 and S100A13 and co-release (Matsunaga and Ueda, 2006a and b). In the present study, we clarified that Cu^{2+} is another regulator that synergistically potentiates the Ca^{2+}-dependent interaction, an initial step in the non-classical release of FGF1, using a biosensor QCM assay.

QCM is a real time-mass measuring device to determine the intermolecular interaction. The interactions were detected as the change in the intrinsic frequency of quartz crystal, due to changes in the mass on the electrode. First we demonstrated the Ca^{2+} concentration–dependency on the interaction between GST-FGF1 and *Strep*-tagII-S100A13, being consistent to the fact that S100A13 possesses EF-hand domain for Ca^{2+}-binding. Although Ca^{2+} alone, but not Mg^{2+} or Cu^{2+} alone caused this interaction, the EC_{50} of Ca^{2+} was as high as 10.11 μM, a concentration, which is not normally expected in the cytosol. When 200 nM Cu^{2+} was added with Ca^{2+}, the EC50 of Ca^{2+} was decreased to 2.07 μM, a concentration, which is expected in the cytosol when the cell is stimulated, e.g. through $G_{q/11}$-coupled receptor. The involvement of Cu^{2+} in the interaction was supported by our previous study, in which the fluorescence resonance energy transfer signal between Venus (YFP)-FGF1 and CFP-S100A13 expressing in NG108-15 hybrid cells was decreased by tetrathiomolybdate, a Cu^{2+} chelating agent (Matsunaga and Ueda, 2006b).

Our previous studies demonstrated that the stress-induced release of FGF1 is mediated through activation of Ca^{2+}-induced Ca^{2+} release (CICR) and a voltage-dependent N-type Ca^{2+} channel (Matsunaga and Ueda, 2006a and b). Both

mechanisms cause Ca^{2+} influx and raise the Ca^{2+} concentration to sub-mM levels at the so-called microdomain area in vicinity of plasma membranes or endoplasmic reticulum (Schneggenburger and Neher, 2000; Verkhratsky, 2002; Bouchard et al., 2003; Schwarz, 2003; Tully and Treistman, 2004; García et al., 2006). However, the present fact that the addition of Cu^{2+} decreased the Ca^{2+} concentration required for the interaction to approximately 2 μM Ca^{2+}, suggests that the interaction does not necessarily occur at the microdomain area. Therefore the involvement of CICR and N-type Ca^{2+} channel activations in the stress-induced FGF1 release may be related to other unidentified mechanisms than the initial interaction between FGF1 and S100A13 (Fig. 6A).

A recent study using NMR (Arnesano et al., 2005) proposed that the addition of Ca^{2+} causes structural activation of S100A13 homodimer, and creates two protrusions of positively charged residues located at the C-terminal end (Fig. 6B), which may facilitate the interaction with an acidic protein, such as FGF1. On the other hand, FGF1 is reported to be homodimerized through the Cu^{2+}–catalyzed oxidation of Cys30 of FGF1, and released upon stress in a non-classical manner (Tarantini et al., 1998; LaVallee et al., 1998; Landriscina et al., 2001a). Thus, it is interesting to speculate that Cu^{2+} bound to S100A13 may stabilize the interaction between FGF1 and S100A13 through oxidation and homodimerization of FGF1 (Fig. 6C).

Amlexanox, an inhibitor of co-release of FGF1 and S100A13, abolished the Cu^{2+}-potentiation of the Ca^{2+}–enhanced interaction between both proteins. Although this inhibitor has been known to bind to the C-terminus of S100A13 (Mouta Carreira et al., 1998; Okada et al., 2002), a recent report demonstrated that it also binds to FGF1, particularly to a locus close to Cys30 of this protein (Rajalingam et al., 2005). These findings may well explain why amlexanox selectively abolished Cu^{2+}-potentiation,

without affecting basal Ca^{2+}–enhancement. These results indicate that amlexanox might prevent S100A13 from functioning as a Cu^{2+}-donor to FGF1 (Cys30).

Thus, it is evident that Cu^{2+} plays a key role in the regulation of this protein-protein interaction. Although the static role of Cu^{2+} in non-classical FGF1 release is proven (Tarantini et al., 1998; LaVallee et al., 1998; Landriscina et al., 2001a), its dynamic regulation is unlikely to be important, since the cellular level may not change upon the stress. However, some genetic diseases are closely related to the deficiency or excess of Cu^{2+}. These include Menkes disease and Wilson disease, which include neurological symptoms (Strausak et al., 2001; Mercer, 2001). It remains to be determined whether these diseases are related to the non-classical release of FGF1 or other molecules. However, copper-chelating therapy for cancer patients is well known in the clinic (Daniel et al., 2004). In addition, there is a report that tetrathiolmolybdate repressed neointimal thickening after vascular injury in the rat, possibly through an inhibition of S100A13-dependent non-classical IL-1α release (Mandinov et al., 2003). It should be noted that S100A13 expression in brain astrocytes is claimed to be a maker of tumor grading and vascularization (Landriscina et al., 2006).

In the present study, we successfully demonstrated that dimeric S100A13 interacts with FGF1 and this interaction occurs at a stoichiometry of 1:1. We have reported that the Ca^{2+}-dependent interaction requires C-terminal basic region of S100A13, since the stress-induced FGF1 release completely disappeared in C6 glioma cells expressing S100A13 Δ88-98 mutant (Matsunaga and Ueda, 2006a), suggesting that this deletion mutant functions as a potent dominant negative regulator for FGF1 release. In the present study, however, we demonstrated that [D:D] homodimer has no potency to interact with FGF1. Therefore, the formation of [F:D] heterodimer, which

still retains 50% of [F:F] homodimer, is presumed to play a major role in the regulation of FGF1 release from the cell over-expressed with deletion mutant. However, this fact is not enough to explain the complete loss of FGF1 release from the cell expressing deletion mutant. Therefore, it may be speculated that the deletion mutant loses the potency to interact with unidentified S100A13 target molecules, involved in the stress-induced FGF1 release.

In conclusion, we describe a new approach to studying the role of divalent cations in protein-protein interactions, using biosensor QCM. Through this study, it was revealed that the synergistic effects of Ca^{2+} and Cu^{2+} play a key role in the interaction between FGF1 and S100A13, which is the initial step in non-classical release of FGF1.

Acknowledgements

We gratefully acknowledge Takeda Pharmaceutical Company Ltd. for providing amlexanox. This work was supported in part by Grants-in-Aid for Scientific Research from the Japanese Ministry of Education, Culture, Sports, Science and Technology (KAKENHI 15390028 and 17790066).

References

Arnesano F., Banci, L., Bertini, I., Fantoni, A., Tenori, L., Viezzoli, M. S., 2005. Structural interplay between calcium(II) and copper(II) binding to S100A13 protein. Angew Chem Int Ed Engl 44, 6341-6344.

Bhattacharya S., Bunick, C. G., Chazin, W. J., 2004. Target selectivity in EF-hand calcium binding proteins. Biochim Biophys Acta 1742, 69-79.

Bouchard R., Pattarini, R., Geiger, J. D., 2003. Presence and functional significance of presynaptic ryanodine receptors. Prog Neurobiol 69, 391-418.

Chan W. Y., Xia, C. L., Dong, D. C., Heizmann, C. W., Yew, D. T., 2003. Differential expression of S100 proteins in the developing human hippocampus and temporal cortex. Microsc Res Tech 60, 600-613.

Cleves A. E., 1997. Protein transports: the nonclassical ins and outs. Curr Biol 7, R318-320.

Daniel K. G., Harbach, R. H., Guida, W. C., Dou, Q. P., 2004. Copper storage diseases: Menkes, Wilsons, and cancer. Front Biosci 9, 2652-2662.

Donato R., 1999. Functional roles of S100 proteins, calcium-binding proteins of the EF-hand type. Biochim Biophys Acta 1450, 191-231.

Friesel R., Maciag, T., 1999. Fibroblast growth factor prototype release and fibroblast growth factor receptor signaling. Thromb Haemost 82, 748-754.

García A. G., García-De-Diego, A. M., Gandía, L., Borges, R., García-Sancho, J., 2006. Calcium signaling and exocytosis in adrenal chromaffin cells. Physiol Rev 86, 1093-1131.

Heizmann C. W., Fritz, G., Schäfer, B. W., 2002. S100 proteins: structure, functions and pathology. Front Biosci 7, d1356-1368.

Jackson A., Tarantini, F., Gamble, S., Friedman, S., Maciag, T., 1995. The release of fibroblast growth factor-1 from NIH 3T3 cells in response to temperature involves the function of cysteine residues. J Biol Chem 270, 33-36.

Landriscina M., Bagalá, C., Mandinova, A., Soldi, R., Micucci, I., Bellum, S., Prudovsky, I., Maciag, T., 2001a. Copper induces the assembly of a multiprotein aggregate implicated in the release of fibroblast growth factor 1 in response to stress. J Biol Chem 276, 25549-25557.

Landriscina M., Schinzari, G., Di Leonardo, G., Quirino, M., Cassano, A., D'Argento, E., Lauriola, L., Scerrati, M., Prudovsky, I., Barone, C., 2006. S100A13, a new marker of angiogenesis in human astrocytic gliomas. J Neurooncol 80, 251-259.

Landriscina M., Soldi, R., Bagalá, C., Micucci, I., Bellum, S., Tarantini, F., Prudovsky, I., Maciag, T., 2001b. S100A13 participates in the release of fibroblast growth factor 1 in response to heat shock in vitro. J Biol Chem 276, 22544-22552.

LaVallee T. M., Tarantini, F., Gamble, S., Mouta Carreira, C., Jackson, A., Maciag, T., 1998. Synaptotagmin-1 is required for fibroblast growth factor-1 release. J Biol Chem 273, 22217-22223.

Mandinov L., Mandinova, A., Kyurkchiev, S., Kyurkchiev, D., Kehayov, I., Kolev, V., Soldi, R., Bagala, C., de Muinck, E. D., Lindner, V., Post, M. J., Simons, M., Bellum, S., Prudovsky, I., Maciag, T., 2003. Copper chelation represses the vascular response to injury. Proc Natl Acad Sci U S A 100, 6700-6705.

Mandinova A., Soldi, R., Graziani, I., Bagala, C., Bellum, S., Landriscina, M., Tarantini, F., Prudovsky, I., Maciag, T., 2003. S100A13 mediates the copper-dependent stress-induced release of IL-1alpha from both human U937 and murine NIH 3T3 cells. J Cell Sci 116, 2687-2696.

Matsunaga H., Ueda, H., 2006a. Evidence for serum-deprivation-induced co-release of FGF-1 and S100A13 from astrocytes. Neurochem Int 49, 294-303.

Matsunaga H., Ueda, H., 2006b. Voltage-Dependent N-Type Ca^{2+} Channel Activity Regulates the Interaction Between FGF-1 and S100A13 for Stress-Induced Non-Vesicular Release. Cell Mol Neurobiol 26, 237-246.

Mercer J. F., 2001. The molecular basis of copper-transport diseases. Trends Mol Med 7, 64-69.

Mouta Carreira C., LaVallee, T. M., Tarantini, F., Jackson, A., Lathrop, J. T., Hampton, B., Burgess, W. H., Maciag, T., 1998. S100A13 is involved in the regulation of fibroblast growth factor-1 and p40 synaptotagmin-1 release in vitro. J Biol Chem 273, 22224-22231.

Nickel W., 2003. The mystery of nonclassical protein secretion. A current view on cargo proteins and potential export routes. Eur J Biochem 270, 2109-2119.

Okada M., Tokumitsu, H., Kubota, Y., Kobayashi, R., 2002. Interaction of S100 proteins with the antiallergic drugs, olopatadine, amlexanox, and cromolyn: identification of putative drug binding sites on S100A1 protein. Biochem Biophys Res Commun 292, 1023-1030.

Osterloh D., Ivanenkov, V. V., Gerke, V., 1998. Hydrophobic residues in the C-terminal region of S100A1 are essential for target protein binding but not for dimerization. Cell Calcium 24, 137-151.

Prudovsky I., Mandinova, A., Soldi, R., Bagala, C., Graziani, I., Landriscina, M., Tarantini, F., Duarte, M., Bellum, S., Doherty, H., Maciag, T., 2003. The non-classical export routes: FGF1 and IL-1alpha point the way. J Cell Sci 116, 4871-4881.

Rajalingam D., Kumar, T. K., Soldi, R., Graziani, I., Prudovsky, I., Yu, C., 2005. Molecular mechanism of inhibition of nonclassical FGF-1 export. Biochemistry 44, 15472-15479.

Reuss B., von Bohlen und Halbach, O., 2003. Fibroblast growth factors and their receptors in the central nervous system. Cell Tissue Res 313, 139-157.

Ridinger K., Schäfer, B. W., Durussel, I., Cox, J. A., Heizmann, C. W., 2000. S100A13. Biochemical characterization and subcellular localization in different cell lines. J Biol Chem 275, 8686-8694.

Schneggenburger R., Neher, E., 2000. Intracellular calcium dependence of transmitter release rates at a fast central synapse. Nature 406, 889-893.

Schwarz T. L., 2003. Release of Neurotransmitters. In: Squire L. R., Bloom F. E., McConnell S. K., Roberts J. L., Spitzer N. C., Zigmond M. J. (Ed.) Fundamental neuroscience. Second Edition, Academic Press, Boston, pp. 197-224.

Shishibori T., Oyama, Y., Matsushita, O., Yamashita, K., Furuichi, H., Okabe, A., Maeta, H., Hata, Y., Kobayashi, R., 1999. Three distinct anti-allergic drugs, amlexanox, cromolyn and tranilast, bind to S100A12 and S100A13 of the S100 protein family. Biochem J 338 (Pt 3), 583-589.

Sivaraja V., Kumar, T. K., Prudovsky, I., Yu, C., 2005. Three-dimensional solution structure of a unique S100 protein. Biochem Biophys Res Commun 335, 1140-1148.

Sivaraja V., Suresh Kumar, T. K., Rajalingam, D., Graziani, I., Prudovsky, I., Yu, C., 2006. Copper Binding Affinity of S100A13, a Key Component of the FGF-1 Non-Classical Copper-Dependent Release Complex. Biophys J 91, 1832-1843.

Strausak D., Mercer, J. F., Dieter, H. H., Stremmel, W., Multhaup, G., 2001. Copper in disorders with neurological symptoms: Alzheimer's, Menkes, and Wilson diseases.

Brain Res Bull 55, 175-185.

Tarantini F., Gamble, S., Jackson, A., Maciag, T., 1995. The cysteine residue responsible for the release of fibroblast growth factor-1 residues in a domain independent of the domain for phosphatidylserine binding. J Biol Chem 270, 29039-29042.

Tarantini F., LaVallee, T., Jackson, A., Gamble, S., Mouta Carreira, C., Garfinkel, S., Burgess, W. H., Maciag, T., 1998. The extravesicular domain of synaptotagmin-1 is released with the latent fibroblast growth factor-1 homodimer in response to heat shock. J Biol Chem 273, 22209-22216.

Tully K., Treistman, S. N., 2004. Distinct intracellular calcium profiles following influx through N- versus L-type calcium channels: role of Ca^{2+}-induced Ca^{2+} release. J Neurophysiol 92, 135-143.

Verkhratsky A., 2002. The endoplasmic reticulum and neuronal calcium signalling. Cell Calcium 32, 393-404.

Zimmer D. B., Wright Sadosky, P., Weber, D. J., 2003. Molecular mechanisms of S100-target protein interactions. Microsc Res Tech 60, 552-559.

Figure Legends

Fig. 1. Interaction between GST-FGF1 and *Strep*-tagII-S100A13 or its deletion mutant. (A) Ca^{2+}-sensitive interaction between GST-FGF1 and *Strep*-tagII-S100A13. Interactions were evaluated by the change in oscillation units (OU: -ΔF in Hz), reflecting the change in the mass on the electrode sensor chip, on which GST-FGF1 had previously been immobilized. A small increase in OU was observed when 200 nM *Strep*-tagII-S100A13 was added to the interaction buffer in the cuvette at time 0. However, a large increase was observed following the addition of 10 – 100 μM Ca^{2+}, while this increase was reversed by 2 mM EGTA. Arrow-heads denote application points. (B) S100A13 deletion mutant. The Δ88-98 mutant retains two Ca^{2+}-binding EF-hand motifs, but lacks the C-terminal basic peptide region. (C) Lack of interaction of GST-FGF1 with *Strep*-tagII-S100A13 Δ88-98 mutant.

Fig. 2. Decreased interaction of GST-FGF1 with *Strep*-tagII-S100A13 heterodimers of full-length protein and C-terminal deletion mutant. (A) Three expected dimers comprising full-length [F] and Δ88-98 mutant [D]. (B) Evidence for the partial interaction activity of Δ88-98 in the presence of full-length *Strep*-tagII-S100A13. (C) Maximum mass level bound to GST-FGF1 in various combinations of full-length *Strep*-tagII-S100A13 [F] and Δ88-98 mutant [D]. An increase by 1 Hz OU_{max} at 30 min is calculated as a molecular mass of 30.38 pg bound to GST-FGF1. Results represent means $\pm$ S.E.M. Numbers indicating gray columns are the weight of bound *Strep*-tagII-S100A13 mutant protein (x 10^{-1} ng). (D) Equilibrium analysis (linear-reciprocal plot) of the interaction of GST-FGF1 and dimeric *Strep*-tagII-S100A13 mutants. All data were derived from triplicate measurements.

Fig. 3. Ca^{2+}-enhanced interaction between GST-FGF1 and *Strep*-tagII-S100A13. (A) Time course of the interaction in the presence of various concentrations of Ca^{2+}. No significant enhancement of the interaction was observed with 500 μM Mg^{2+} or 200 nM Cu^{2+}. (B) Ca^{2+}-concentration dependent curve. The OU value was determined at 10 min. This plot fitted to the logarithmic curve used for Michaelis-Menten kinetics (y = 25.371 LOG[x] + 16.176). (C) Hanes-Woolf plot. Each data point in (B) was used for this kinetic analysis. The linear curve is represented by the following formula, y = 0.012[x] + 0.173. The EC_{50} (10.11 μM) of Ca^{2+} for GST-FGF1– *Strep*-tagII-S100A13 interaction was determined by the formula in (B), using OU_{50} (41.67), which is calculated as 0.5 x OU_{max} (83.33). (D) Cumulative application of *Strep*-tagII-S100A13 in the presence of 100 μM Ca^{2+}. Arrow-heads denote application points of *Strep*-tagII-S100A13 (final concentration: 12.5 – 425 nM). (E) Kinetic analysis of the Ca^{2+} requirement for the FGF1-S100A13 interaction. The $1/\tau$ value from the cumulative *Strep*-tagII-S100A13 application-induced OU change in (D) was plotted against each concentration (12.5 – 425 nM) and this plot was fitted to a linear curve. A slope and intercept denote k_a and k_d, respectively. k_d/k_a represents K_D value. (F and G) The k_a and K_D values for the Ca^{2+}-enhanced interaction between GST-FGF1 and *Strep*-tagII-S100A13. The data shown are means ± S.E.M. $*p < 0.01$ *vs.* none (Student's *t*-test). All data were derived from triplicate measurements.

Fig. 4. Potentiation of the Ca^{2+}-enhanced interaction between GST-FGF1 and *Strep*-tagII-S100A13 by Cu^{2+}. (A) Time course of interaction in the presence of various concentrations of Cu^{2+}. Results represent data under the condition of a high concentration (100 μM) of Ca^{2+}. (B) Cu^{2+} concentration-dependent potentiation of the interaction. The OU represents the difference between the presence and absence of Cu^{2+} at 10 min. (C) Hanes-Woolf plot. The EC_{50} of Cu^{2+} for potentiation was 50.45 nM. (D) Ca^{2+} concentration-response curve for the GST-FGF1 - *Strep*-tagII-S100A13 interaction in the presence or absence of Cu^{2+}. (E) Hanes-Woolf plot. Each data point in (D) was used for this kinetic analysis. The EC_{50} of Ca^{2+} was 2.07 or 11.69 μM in the presence or absence of Cu^{2+}, respectively. All data were derived from triplicate measurements.

Fig. 5. Amlexanox-induced inhibition of the interaction between GST-FGF1 and *Strep*-tagII-S100A13. (A) Amlexanox concentration-dependent increase in K_D values for the interaction. The data shown are means ± S.E.M. *$p < 0.05$ and **$p < 0.01$ *vs.* the absence of amlexanox (Student's *t*-test). (B) Dixon plot. Relaxation time (τ) values were plotted against different concentrations of amlexanox (0, 0.1, 1 and 3 μM). Linear-curves show an intersection point, and this x-coordinate represents - K_i. Arrow denotes an intersection point. Data were derived from triplicate measurements. All experiments were analyzed in interaction buffer containing 500 μM Mg^{2+}, 100 μM Ca^{2+} and 200 nM Cu^{2+}.

Fig. 6. Ca^{2+} and Cu^{2+}-involvements of FGF1-S100A13 interaction. (A) FGF1-S100A13 interaction in the cytosol. Microdomain is the area containing sub-mM levels of Ca^{2+} in the vicinity of membrane voltage-dependent N-type Ca^{2+} channel and ryanodine receptor in the endoplasmic reticulum (ER). The Ca^{2+} level in the cytosol, where the interaction between FGF1 and Cu^{2+}-bound S100A13 is presumed to occur, is below 2 μM in the activated cell. (B and C) Schematic model for structural interplay between Ca^{2+} and Cu^{2+} binding in the formation of the FGF1-S100A13 complex. (B) Proposed model for the Ca^{2+}-induced conformational change of dimeric S100A13 (*Homo sapiens*). The model represents vertical views of the electrostatic potential surface of apo-S100A13 (Protein Data Bank: 1YUS) and Ca^{2+}-S100A13 (1YUU). The negative to positive potential charged amino acids are represented in a blue to red gradient color. A positively charged cluster was located at the C-terminal end of S100A13 (arrows). (C) A hypothetical model for Cu^{2+}-regulated interaction between FGF1 and S100A13. The model represents a ribbon representation of the interaction between FGF1 (*Homo sapiens*, Protein Data Bank: 2ERM) and S100A13, and its regulation by Ca^{2+} and Cu^{2+}. The potential Cu^{2+}-binding residues of Ca^{2+}-S100A13 are represented as yellow wires (Glu4, Glu8, Glu11 and His48'). In the hypothesis, Ca^{2+} enhances the interaction between FGF1 and S100A13. In the presence of Ca^{2+}, two Cu^{2+} ions bind to the S100A13 dimer, which in turn oxidizes the Cys30 residue of FGF1 as a Cu^{2+} donor. The resulting disulfide bond between two FGF1 molecules may potentiate the Ca^{2+}-enhanced interaction between FGF1 and S100A13. Ca^{2+} and Cu^{2+} are represented as orange and blue spheres, respectively. 3D structures were analyzed by iMol software.

Table

Table 1. The association rate constant (k_a) and dissociation constant (K_D) value of S100A13 for FGF1.

	Ca^{2+} (M)	Cu^{2+} (200 nM)	Amlexanox (μM)	k_a (10^4 $M^{-1}s^{-1}$)		K_D (10^{-7} M)	
A	10^{-7}	-	0	9.53 ± 0.20		5.36 ± 0.16	
B	10^{-4}	-	0	40.3 ± 0.49	**	0.75 ± 0.01	**
C	10^{-7}	+	0	8.49 ± 0.36		4.72 ± 0.18	
D	10^{-4}	+	0	55.0 ± 0.56	**##	0.38 ± 0.01	**#
E	10^{-7}	-	0	1.67 ± 0.36		5.19 ± 1.16	
F	10^{-4}	-	0	9.48 ± 0.37	**	0.21 ± 0.01	*
G	10^{-4}	+	0	15.2 ± 0.65	##	0.13 ± 0.01	
H	10^{-4}	-	100	39.7 ± 0.34		0.76 ± 0.01	
I	10^{-4}	+	100	42.9 ± 0.51	†	0.71 ± 0.01	†

The interaction between FGF-1 and S100A13 was enhanced by the further addition of Ca^{2+} and potentiated by the addition of Cu^{2+}. A–D and H–I: The interaction was analyzed by both GST-FGF1 and *Strep*-tagII-S100A13. GST-FGF1 was immobilized on the anti-GST antibody coated sensor chip, hence orientation of FGF-1 (host sample) was fixed. k_a and K_D were obtained by the analysis using cumulative application of recombinant S100A13 protein (guest sample). E–G: The FGF1-S100A13 interaction was analyzed by using tag-free recombinant proteins. Tag-free FGF1 was directly immobilized on sensor chip. The Cu^{2+}–induced potentiation of this interaction was abolished by amlexanox. Each experiment was analyzed in 500 μM $MgCl_2$-containing interaction buffer. The data shown are means ± S.E.M. *$p < 0.05$ and **$p < 0.01$ *vs*. corresponding control (A, C and E). #$p < 0.05$ and ##$p < 0.01$ *vs*. corresponding free of Cu^{2+} (B and F). †$p < 0.01$ *vs*. D. All significant differences were analyzed by Dunnett's multiple comparison test.

Figures

Figure 1

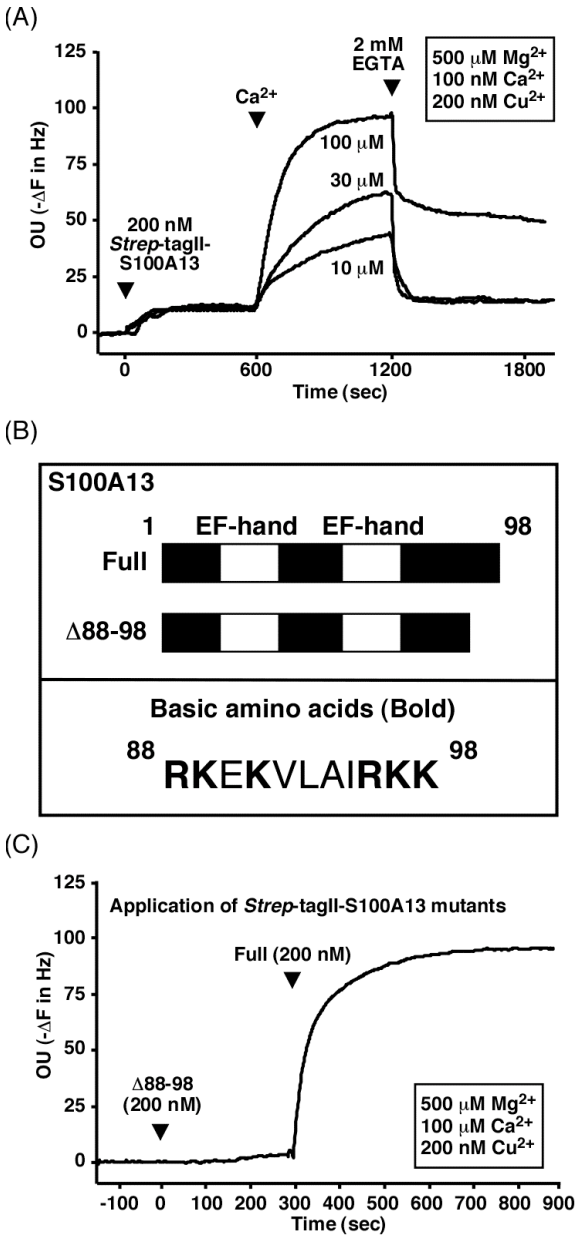

Figure 2

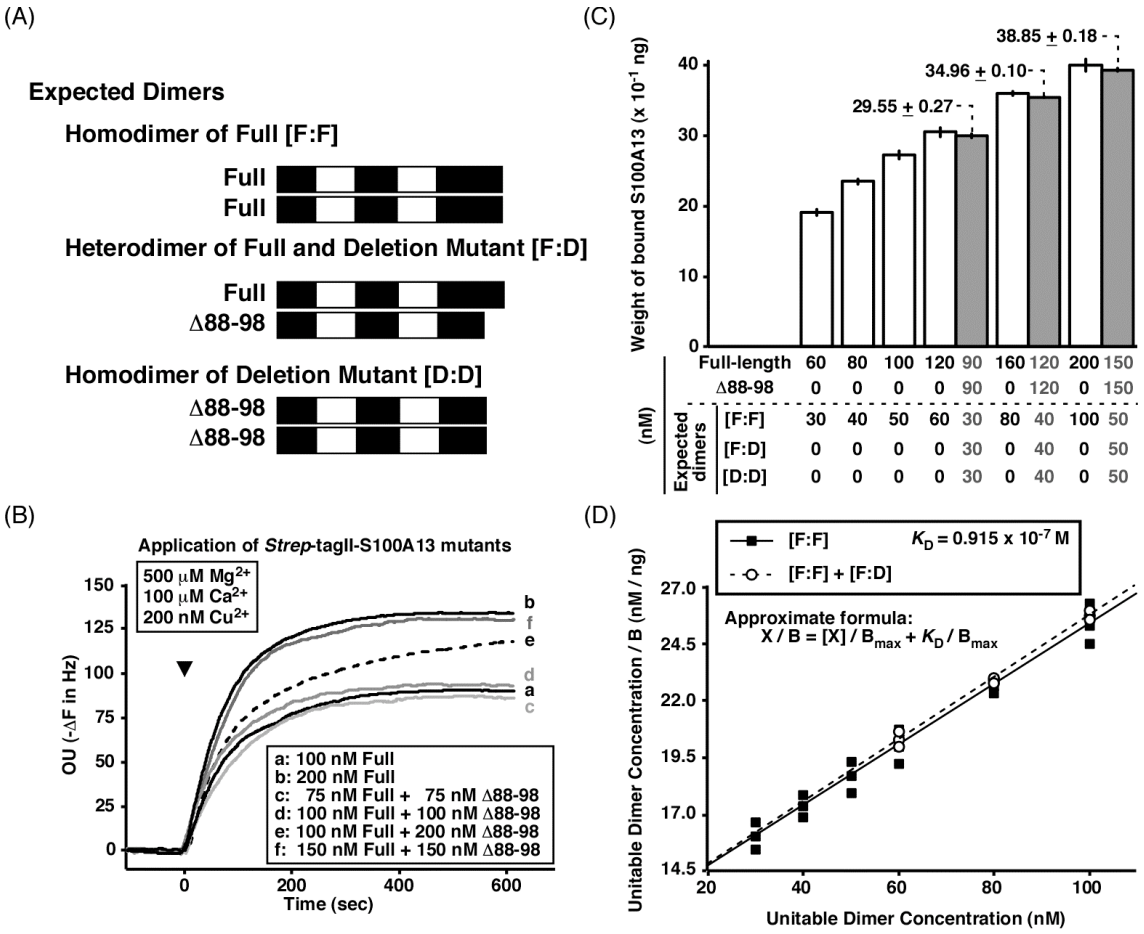
(A)
Expected Dimers
Homodimer of Full [F:F]
Full
Full
Heterodimer of Full and Deletion Mutant [F:D]
Full
Δ88-98
Homodimer of Deletion Mutant [D:D]
Δ88-98
Δ88-98
(B)
Application of Strep-tagII-S100A13 mutants
500 μM Mg2+
100 μM Ca2+
200 nM Cu2+
OU (-ΔF in Hz)
Time (sec)
a: 100 nM Full
b: 200 nM Full
c: 75 nM Full + 75 nM Δ88-98
d: 100 nM Full + 100 nM Δ88-98
e: 100 nM Full + 200 nM Δ88-98
f: 150 nM Full + 150 nM Δ88-98
(C)
Weight of bound S100A13 (x 10-1 ng)
38.85 ± 0.18
34.96 ± 0.10
29.55 ± 0.27
Full-length 60 80 100 120 90 160 120 200 150
Δ88-98 0 0 0 0 90 0 120 0 150
(nM)
Expected dimers
[F:F] 30 40 50 60 30 80 40 100 50
[F:D] 0 0 0 0 30 0 40 0 50
[D:D] 0 0 0 0 30 0 40 0 50
(D)
[F:F] KD = 0.915 x 10-7 M
[F:F] + [F:D]
Approximate formula:
X / B = [X] / Bmax + KD / Bmax
Unitable Dimer Concentration / B (nM / ng)
Unitable Dimer Concentration (nM)

Figure 3

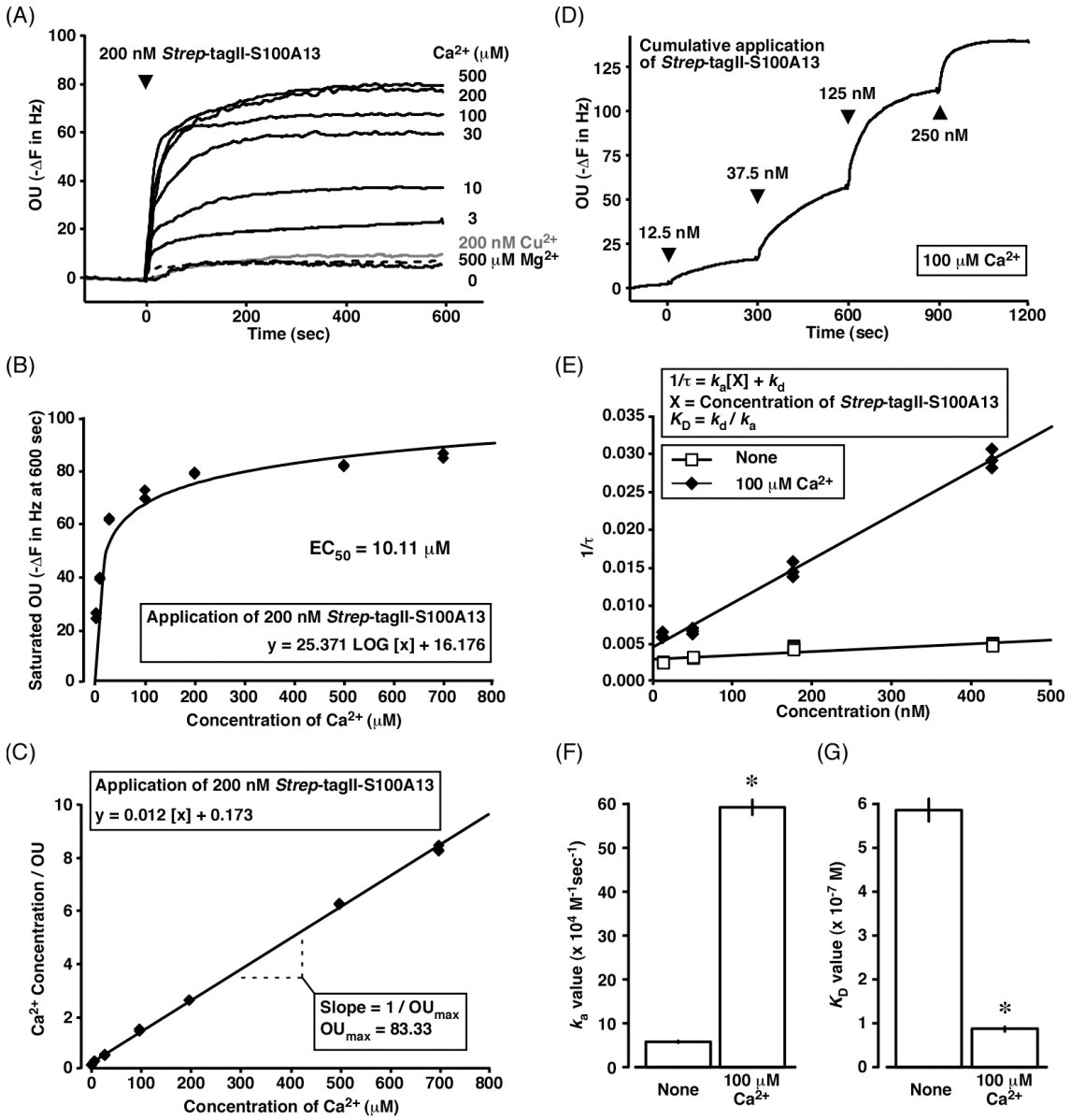
(A)
200 nM Strep-tagII-S100A13
Ca2+ (μM)
500
200
100
30
10
3
200 nM Cu2+
500 μM Mg2+
0
OU (-ΔF in Hz)
Time (sec)
(B)
Saturated OU (-ΔF in Hz at 600 sec)
EC50 = 10.11 μM
Application of 200 nM Strep-tagII-S100A13
y = 25.371 LOG [x] + 16.176
Concentration of Ca2+ (μM)
(C)
Application of 200 nM Strep-tagII-S100A13
y = 0.012 [x] + 0.173
Slope = 1 / OUmax
OUmax = 83.33
Ca2+ Concentration / OU
Concentration of Ca2+ (μM)
(D)
Cumulative application of Strep-tagII-S100A13
12.5 nM
37.5 nM
125 nM
250 nM
100 μM Ca2+
OU (-ΔF in Hz)
Time (sec)
(E)
1/τ = ka[X] + kd
X = Concentration of Strep-tagII-S100A13
KD = kd / ka
None
100 μM Ca2+
1/τ
Concentration (nM)
(F)
ka value (x 10^4 M^-1sec^-1)
None
100 μM Ca2+
(G)
KD value (x 10^-7 M)
None
100 μM Ca2+

Figure 4

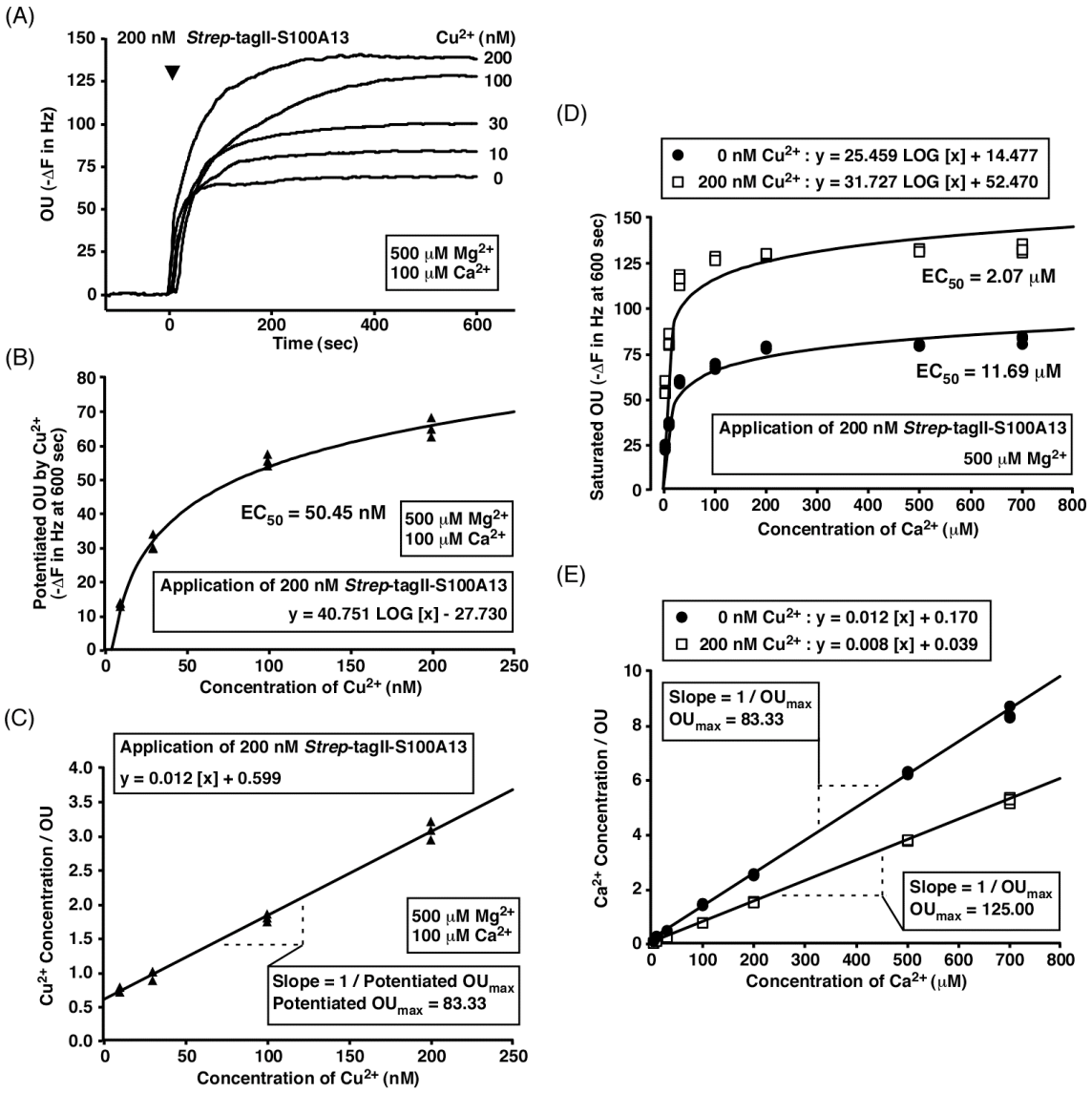
(A)
200 nM Strep-tagII-S100A13
Cu2+ (nM)
200
100
30
10
0
500 μM Mg2+
100 μM Ca2+
OU (-ΔF in Hz)
Time (sec)
(B)
EC50 = 50.45 nM
500 μM Mg2+
100 μM Ca2+
Application of 200 nM Strep-tagII-S100A13
y = 40.751 LOG [x] - 27.730
Potentiated OU by Cu2+ (-ΔF in Hz at 600 sec)
Concentration of Cu2+ (nM)
(C)
Application of 200 nM Strep-tagII-S100A13
y = 0.012 [x] + 0.599
500 μM Mg2+
100 μM Ca2+
Slope = 1 / Potentiated OUmax
Potentiated OUmax = 83.33
Cu2+ Concentration / OU
Concentration of Cu2+ (nM)
(D)
0 nM Cu2+ : y = 25.459 LOG [x] + 14.477
200 nM Cu2+ : y = 31.727 LOG [x] + 52.470
EC50 = 2.07 μM
EC50 = 11.69 μM
Application of 200 nM Strep-tagII-S100A13
500 μM Mg2+
Saturated OU (-ΔF in Hz at 600 sec)
Concentration of Ca2+ (μM)
(E)
0 nM Cu2+ : y = 0.012 [x] + 0.170
200 nM Cu2+ : y = 0.008 [x] + 0.039
Slope = 1 / OUmax
OUmax = 83.33
Slope = 1 / OUmax
OUmax = 125.00
Ca2+ Concentration / OU
Concentration of Ca2+ (μM)

Figure 5

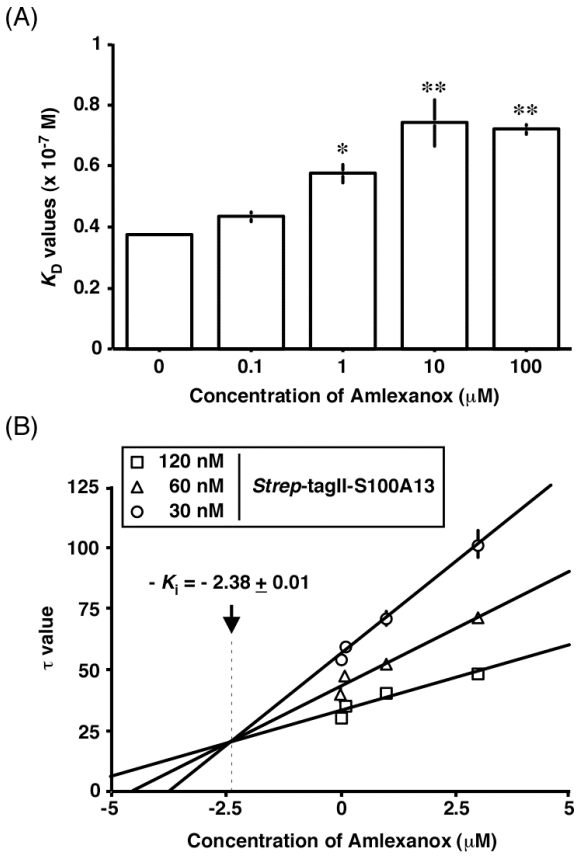
(A)
K_D values (x 10^{-7} M)
1
0.8
0.6
0.4
0.2
0
*
**
**
0
0.1
1
10
100
Concentration of Amlexanox (μM)
(B)
120 nM
60 nM
30 nM
Strep-tagII-S100A13
- K_i = - 2.38 ± 0.01
τ value
125
100
75
50
25
0
-5
-2.5
0
2.5
5
Concentration of Amlexanox (μM)

Figure 6

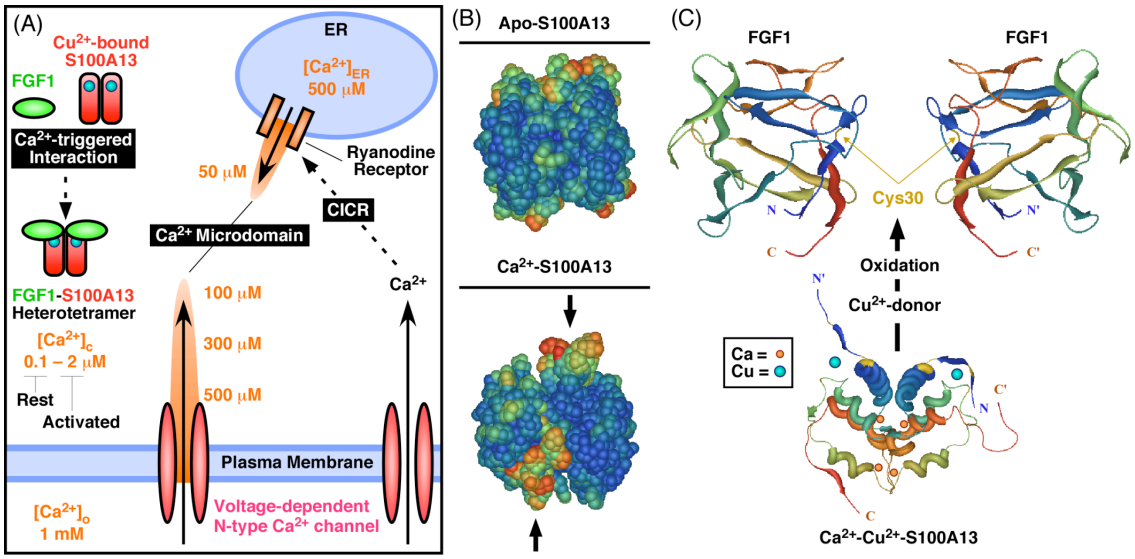
(A)
Cu2+-bound S100A13
FGF1
Ca2+-triggered Interaction
FGF1-S100A13 Heterotetramer
[Ca2+]c 0.1 – 2 μM
Rest
Activated
ER
[Ca2+]ER 500 μM
Ryanodine Receptor
50 μM
CICR
Ca2+ Microdomain
Ca2+
100 μM
300 μM
500 μM
Plasma Membrane
[Ca2+]o 1 mM
Voltage-dependent N-type Ca2+ channel
(B)
Apo-S100A13
Ca2+-S100A13
(C)
FGF1
FGF1
Cys30
Oxidation
Cu2+-donor
Ca =
Cu =
Ca2+-Cu2+-S100A13